



Measurement of the generalized spin polarizabilities of the neutron in the low-Q² region

Vincent Sulkosky^{1,2,3}, Chao Peng^{4,5}, Jian-ping Chen², Alexandre Deur ^{10,2,3 ⋈}, Sergev Abrahamvan⁶. Konrad A. Anjol⁷, David S. Armstrong 10, Todd Averett¹, Stephen J. Bailev¹, Arje Beck⁸, Pierre Bertin⁹, Florentin Butaru¹⁰, Werner Boeglin¹¹, Alexandre Camsonne⁹, Gordon D. Cates ¹⁰, Chia-Cheh Chang¹², Seonho Choi¹⁰, Eugene Chudakov², Luminita Coman¹¹, Juan C. Cornejo ¹⁰, Brandon Craver³, Francesco Cusanno¹³, Raffaele De Leo¹⁴, Cornelis W. de Jager^{2,35}, Joseph D. Denton¹⁵, Seema Dhamija¹⁶, Robert Feuerbach², John M. Finn^{1,35}, Salvatore Frullani^{13,17,35}, Kirsten Fuoti¹, Haiyan Gao 64, Franco Garibaldi 13,17, Olivier Gayou8, Ronald Gilman 2,18, Alexander Glamazdin 19, Charles Glashausser¹⁸, Javier Gomez², Jens-Ole Hansen², David Hayes²⁰, F. William Hersman²¹, Douglas W. Higinbotham ¹, Timothy Holmstrom T, Thomas B. Humensky Charles E. Hyde C, Timothy Holmstrom D, Thomas B. Humensky Charles E. Hyde C, Timothy Holmstrom D, Thomas B. Humensky C, Timothy Holmstrom D, Thomas B. Humensky C, Timothy Holmstrom D, Thomas B. Humensky C, Timothy Holmstrom D, Timothy Holmstrom D, Thomas B. Humensky C, Timothy Holmstrom D, Timoth Hassan Ibrahim^{20,22}, Mauro Iodice¹³, Xiandong Jiang¹⁸, Lisa J. Kaufman²³, Aidan Kelleher¹, Kathryn E. Keister¹, Wooyoung Kim²⁴, Ameya Kolarkar¹⁶, Norm Kolb²⁵, Wolfgang Korsch¹⁶, Kevin Kramer^{1,4}, Gerfried Kumbartzki¹⁸, Luigi Lagamba¹⁴, Vivien Lainé^{2,9}, Geraud Laveissiere⁹, John J. Lerose², David Lhuillier²⁶, Richard Lindgren³, Nilanga Liyanage^{2,3}, Hai-Jiang Lu²⁷, Bin Ma⁸, Demetrius J. Margaziotis⁷, Peter Markowitz¹¹, Kathleen R. McCormick¹⁸, Mehdi Meziane^{1,4}, Zein-Eddine Meziani¹⁰, Robert Michaels², Bryan Moffit¹, Peter Monaghan⁸, Sirish Nanda², Jennifer Niedziela²³, Mikhail Niskin¹¹, Ronald Pandolfi²⁸, Kent D. Paschke²³, Milan Potokar^{29,35}, Andrew Puckett ¹⁰³, Vina A. Punjabi³⁰, Yi Qiang ¹⁰⁸, Ronald D. Ransome¹⁸, Bodo Reitz², Rikki Roché³¹, Arun Saha^{2,35}, Alexander Shabetai¹⁸, Simon Širca³², Jaideep T. Singh³, Karl Slifer¹⁰, Ryan Snyder³, Patricia Solvignon^{10,35}, Robert Stringer⁴, Ramesh Subedi^{33,35}, William A. Tobias³, Ngyen Ton³, Paul E. Ulmer²⁰, Guido Maria Urciuoli¹³, Antonin Vacheret²⁶, Eric Voutier³⁴, Kebin Wang³, Lu Wan⁸, Bogdan Wojtsekhowski^{©2}, Seungtae Woo²⁴, Huan Yao¹⁰, Jing Yuan¹⁸, Xiaohui Zhan⁸, Xiaochao Zheng 10 3,5 and Lingyan Zhu⁸

Understanding the nucleon spin structure in the regime where the strong interaction becomes truly strong poses a challenge to both experiment and theory. At energy scales below the nucleon mass of about 1 GeV, the intense interaction among the quarks and gluons inside the nucleon makes them highly correlated. Their coherent behaviour causes the emergence of effective degrees of freedom, requiring the application of non-perturbative techniques such as chiral effective field theory1. Here we present measurements of the neutron's generalized spin polarizabilities that quantify the neutron's spin precession under electromagnetic fields at very low energy-momentum transfer squared down to 0.035 GeV2. In this regime, chiral effective field theory calculations²⁻⁴ are expected to be applicable. Our data, however, show a strong discrepancy with these predictions, presenting a challenge to the current description of the neutron's spin properties.

The nucleon is the basic building block of nature, accounting for about 99% of the universe's visible mass. Understanding its properties, for example, mass and spin, is therefore crucial. Those are mainly determined by the strong interaction, which is described by quantum chromodynamics (QCD) with quarks and gluons as the fundamental degrees of freedom. The nucleon structure is satisfactorily understood at high Q2 (short space-time scales; see Fig. 1 for the definition of kinematic variables), because there QCD is calculable using perturbation methods (perturbative QCD) and tested by numerous experimental measurements. At lower Q^2 , the strong coupling α_s becomes too large for perturbative QCD to be applicable⁵. Yet, calculations are critically needed because the strong interaction's chiral symmetry breaks in this region. Chiral symmetry and its breaking is one of the most important properties of the strong interaction and is believed to lead to the emergence of the nucleon's global properties. To understand how the underlying structure leads to the emergence of LETTERS NATURE PHYSICS

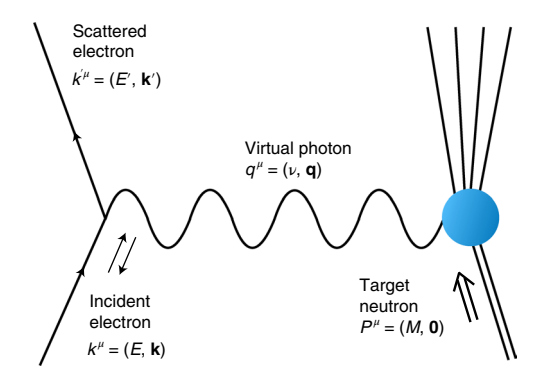


Fig. 1 | **Electron scattering off a neutron by the one-photon exchange process.** The four-momenta of the incident and the scattered electrons are $k^{\mu} = (E, \mathbf{k})$ and $k'^{\mu} = (E', \mathbf{k}')$, respectively, and that of the photon is $q^{\mu} = (\nu, \mathbf{q})$. The neutron, at rest in the laboratory frame, has a four-momentum $P^{\mu} = (M, \mathbf{0})$. The arrows $\uparrow \downarrow$ represent the spin direction of the incident electron and \Uparrow that of the neutron. The generalized spin polarizabilities of the neutron can be measured when both the incident electron and the neutron are polarized.

these global properties, non-perturbative methods must be used. A method using the fundamental quark and gluon degrees of freedom is lattice QCD. However, calculations from this method are often intractable for spin observables at low Q2 (ref. 6). Another solution is to employ effective theories. Chiral effective field theory (yEFT) capitalizes on QCD's approximate chiral symmetry and uses the emergent hadronic degrees of freedom. Therein lies χ EFT's strengths and challenges: although the nucleon and the pion are used for first-order calculations, this is often insufficient to describe the data, and heavier hadrons, such as the nucleon's first excited state $\Delta(1232)$, become needed. This complicates γ EFT calculations, and theorists are still seeking the best way to include the $\Delta(1232)$ in their calculations. It is therefore crucial to perform precision measurements at low enough Q² to test χEFT calculations. Spin observables, among them the generalized spin polarizabilities that are reported here, provide an extensive set of tests to benchmark xEFT calculations⁶.

Polarizabilities describe how the components of an object collectively react to external electromagnetic fields. In particular, spin polarizabilities quantify the object's spin precession under an electromagnetic field. The spin polarizabilities, initially defined with real photons, can be generalized to virtual photons such as those used to probe the neutron in our experiment. Accordingly, generalized spin polarizabilities are extracted by scattering polarized electrons off polarized nucleons and measuring how the cross-section changes when the relative orientation between the electron and nucleon spins is varied (Fig. 1). The energy-momentum transferred between the electron and neutron is (ν, \mathbf{q}) , with $Q^2 = \mathbf{q}^2 - \nu^2$ characterizing the space-time scale at which we probe the neutron. Whereas real photons ($Q^2 = 0$) have only transverse polarizations, mediating virtual photons $(Q^2 \neq 0)$ are transversely (T) or longitudinally (L) polarized. Thus, two contributions to the spin polarizability arise: one from the transverse-transverse (TT) interference called the forward spin polarizability $\gamma_0(Q^2)$, and the other from the longitudinal-transverse (LT) interference, called the longitudinal-transverse interference polarizability $\delta_{LT}(Q^2)$, which is available only with virtual photons. The additional longitudinal polarization direction and the ensuing interference term offer extra latitude to test theories describing the strong interaction.

The theoretical basis to measure $\delta_{LT}(Q^2)$ originates from a work of Gell-Mann, Goldberger and Thirring^{7,8}. This work led to relations

between the cross-sections measured in polarized electron–nucleon scattering (Fig. 1) and the spin polarizabilities:

$$\gamma_0(Q^2) = \frac{1}{2\pi^2} \int_{\nu_0}^{\infty} \frac{\kappa_{\gamma}}{\nu^2} \frac{\sigma_{\text{TT}}(\nu, Q^2)}{\nu^2} d\nu,$$
 (1)

$$\delta_{\mathrm{LT}}(Q^2) = \left(\frac{1}{2\pi^2}\right) \int_{\nu_0}^{\infty} \frac{\kappa_{\gamma}}{\nu Q} \frac{\sigma_{\mathrm{LT}}(\nu, Q^2)}{\nu^2} \mathrm{d}\nu,$$
 (2)

where $\kappa_{\gamma} = \nu - \frac{Q^2}{2M}$ (ref. ⁹) is the photon flux factor, ν_0 is the photo-production threshold and $\sigma_{\rm TT}$ and $\sigma_{\rm LT}$ are the TT and LT interference cross-sections, respectively. The cross-sections are obtained from ^{6,10}

$$\begin{split} \sigma_{\mathrm{TT}}(\nu,Q^2) &= \frac{\pi^2 E Q^2 (1-\varepsilon)}{\alpha \kappa_{\gamma} E' (1-\varepsilon E'/E) (1+\eta \zeta)} \\ &\left(\sqrt{\frac{2\varepsilon}{1+\varepsilon}} \Delta \sigma_{\parallel}(\nu,Q^2) - \eta \Delta \sigma_{\perp}(\nu,Q^2) \right), \end{split} \tag{3}$$

$$\begin{split} \sigma_{\mathrm{LT}}(\nu,Q^2) &= \frac{\pi^2 E Q^2 (1-\varepsilon)}{\alpha \kappa_{\gamma} E' (1-\varepsilon E'/E) (1+\eta \zeta)} \\ &\left(\sqrt{\frac{2\varepsilon}{1+\varepsilon}} \zeta \Delta \sigma_{\parallel}(\nu,Q^2) + \Delta \sigma_{\perp}(\nu,Q^2) \right), \end{split} \tag{4}$$

where $\Delta\sigma_{\parallel}$ ($\Delta\sigma_{\perp}$) is the difference between the cross-sections when the beam and target spin directions are parallel and antiparallel (perpendicular), α is the electromagnetic coupling constant, $\varepsilon=1/[1+2(1+\frac{Q^2}{4M^2x^2})\tan^2(\frac{\theta}{2})]$ with $x=\frac{Q^2}{2m\nu}$ the Bjorken scaling variable and θ the electron scattering angle in the laboratory frame, $\eta=\frac{\varepsilon Q}{(E-E'\varepsilon)}$ and $\zeta=\frac{\eta(1+\varepsilon)}{2\varepsilon}$. The $\sigma_{\rm TT}$ and $\sigma_{\rm LT}$ (Figs. 2 and 3) were integrated according to equations (1) and (2) to obtain $\gamma_0(Q^2)$ and $\delta_{\rm LT}(Q^2)$. The unmeasured part of the integrals at large ν is often negligible owing to the ν weighting.

An outstanding feature of $\delta_{LT}(Q^2)$ at low Q^2 is that the $\Delta(1232)$ is not expected to contribute appreciably to the LT interference cross-section, because excitation of the $\Delta(1232)$ overwhelmingly involves transverse photons. This should alleviate the difficulty of including the $\Delta(1232)$ in χ EFT calculations, making them more robust. However, the first measurement of $\delta_{LT}(Q^2)$ from Jefferson Lab (JLab) experiment E94-010 (ref. 11) done at $Q^2 \geq 0.1\,\text{GeV}^2$ strongly disagreed with χ EFT calculations 12,13 . This surprising result, known as the ' δ_{LT} puzzle' triggered improved χ EFT calculations that now explicitly include the $\Delta(1232)$ (ref. $^{2-4}$), and measurements of δ_{LT} at lower Q^2 where χ EFT can be best tested. New data of δ_{LT} on the neutron at very low Q^2 , which were taken during experiment JLab E97-110, are presented next.

Equation (2) allows the measurement of $\delta_{LT}^n(Q^2)$ (where the superscript n indicates neutron quantities) by scattering polarized electrons off polarized neutrons in ³He nuclei. The data were acquired in Hall A¹⁵ of JLab during experiment E97-110 (ref. ¹⁶). The probing virtual photons were produced by a longitudinally polarized electron beam during its scattering off a polarized ³He target15. The beam polarization, flipped pseudo-randomly at 30 Hz and monitored by Møller and Compton polarimeters, was (75.0 ± 2.3) %. The beam energies ranged from 1.1 GeV to 4.4 GeV and the beam current was typically a few µA. As free neutrons are unstable, we used ³He nuclei as an effective polarized neutron target. To first order, polarized ³He nuclei can be treated as effective polarized neutrons together with unpolarized protons because the ³He nucleons (two protons and one neutron) are mostly in an S state, and so the Pauli exclusion principle dictates that in the S state the proton spins point oppositely, yielding no net contribution to the 3He spin. The gaseous (~12 atm) 3He was contained in a 40-cm-long glass cylinder and polarized by spin-exchange optical

NATURE PHYSICS LETTERS

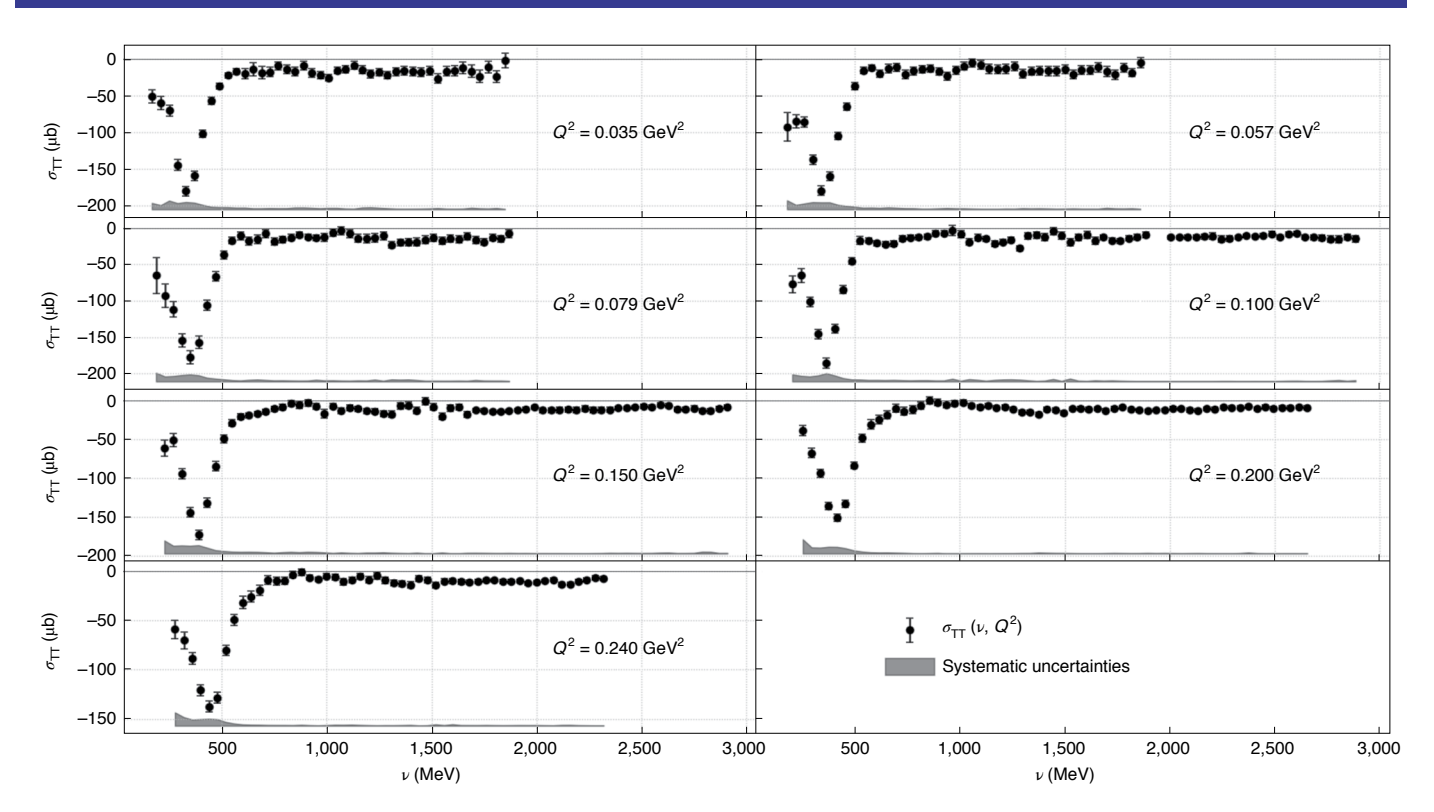


Fig. 2 | The transverse-transverse cross-section $\sigma_{TT}(\nu, Q^2)$ for 3 He. The data are displayed at the Q^2 values at which they are integrated to form γ_0 (equation (1)). The error bars, sometimes too small to be visible, represent the statistical uncertainties. The systematic uncertainty is indicated by the band at the bottom of each panel. The nuclear corrections providing the neutron information from the 3 He data are applied after the integration. The prominent negative peak at small ν is the Δ (1232) contribution.

pumping of rubidium atoms. Helmholtz coils provided a longitudinal or transverse 2.5 mT field used to maintain the polarization, to orient it longitudinally or transversely (in-plane) to the beam direction and to aid in performing polarimetry. The average target polarization in-beam was (39.0 \pm 1.6)%. The scattered electrons from the reaction $^3\overline{\text{He}}(\overrightarrow{e},e')$ were detected by a high-resolution spectrometer supplemented by a dipole magnet , which allowed us to detect electrons scattered at angles down to 6°. Behind the high-resolution spectrometer, drift chambers provided particle tracking, scintillator planes enabled the data acquisition trigger, and a gas Cherenkov counter and electromagnetic calorimeters ensured the identification of the particle type.

The measured σ_{TT} (σ_{IT}) on ³He is shown in Fig. 2 (Fig. 3). Its values with their uncertainties are available in the Supplementary Information. Although polarized ³He nuclei are effectively polarized neutrons to good approximation, nuclear corrections are needed to obtain genuine neutron information. The prescription of ref. 18 was used for the correction. The effect of the nuclear correction, which can be obtained from Supplementary Tables 1-3, is relatively small. In particular it does not appreciably affect the Q² trend seen for the uncorrected ³He integrals. The relative uncertainty on this correction is estimated to be 6% to 14% relative to the correction, the higher uncertainties corresponding to our lowest Q² values. The quasi-elastic contamination was corrected following the procedure described in ref. ¹⁶. The correction is small for δ_{LT}^n but important for γ_0^n and was estimated using ref. ¹⁹. No calculation uncertainty is provided in ref. 19 and using another quasi-elastic calculation 20 may shift the lowest- $Q^2 \gamma_0^n$ data points by as much as our total systematic uncertainty. The other main systematic uncertainties come from the absolute cross-sections (3.5% to 4.5%), target and beam polarizations (3% to 5% and 3.5%, respectively) and radiative corrections (3% to 7%).

Our $\delta_{1T}^n(Q^2)$ data are shown in the left panel of Fig. 4. They agree with earlier data from E94-010 at larger O2 (ref. 11) and reach much lower Q2 where the xEFT is expected to work well. The measurement results can be compared to those of χΕFT calculations^{2,4,12,13} and of a model parameterization of the world photo-production and electro-production data called MAID21. Earlier xEFT calculations^{12,13} used different approaches (heavy baryon and relativistic baryon chiral perturbation theory, or HBγPT and RBγPT, respectively), and furthermore they either neglected the $\Delta(1232)$ degrees of freedom or included it approximately. Newer calculations²⁻⁴, which are all fully relativistic, account for the $\Delta(1232)$ explicitly by using a perturbative expansion, but they differ in their choice of expansion parameter. Despite this theoretical improvement and the small-Q² reach that places our data well in the validity domain of χ EFT, our $\delta_{LT}^n(Q^2)$ starkly disagrees with the predictions. This is even more surprising because the latest χ EFT calculations of δ_{1T}^n agree with each other, suggesting that calculations for this particular observable should be under control. However, our data reveal an opposite trend with Q^2 to that of all the χ EFT calculations.

This startling discrepancy demanded further scrutiny of our data. They are compatible with the E94-010 data where they overlap. This is also true for $\gamma_0^n(Q^2)$, which we measured concurrently and show in the right panel of Fig. 4. The measured $\gamma_0^n(Q^2)$ data also agree with data from experiment EG1 of the Continuous Electron Beam Accelerator Facility (CEBAF) large acceptance spectrometer (CLAS)²², for which a target and detectors were used that are very different from those of E97-110 and E94-010. Our $\gamma_0^n(Q^2)$ data generally disagree with χ EFT calculations. As $\gamma_0(Q^2)$ does not benefit from the suppression of the $\Delta(1232)$ contribution, and as $\gamma_0^n(Q^2)$ predictions do not reach a consensus, this disagreement is not entirely surprising, in contrast to the unexpected $\delta_{\rm LT}^n(Q^2)$ disagreement. Interestingly, we can also study with our data the Schwinger

LETTERS NATURE PHYSICS

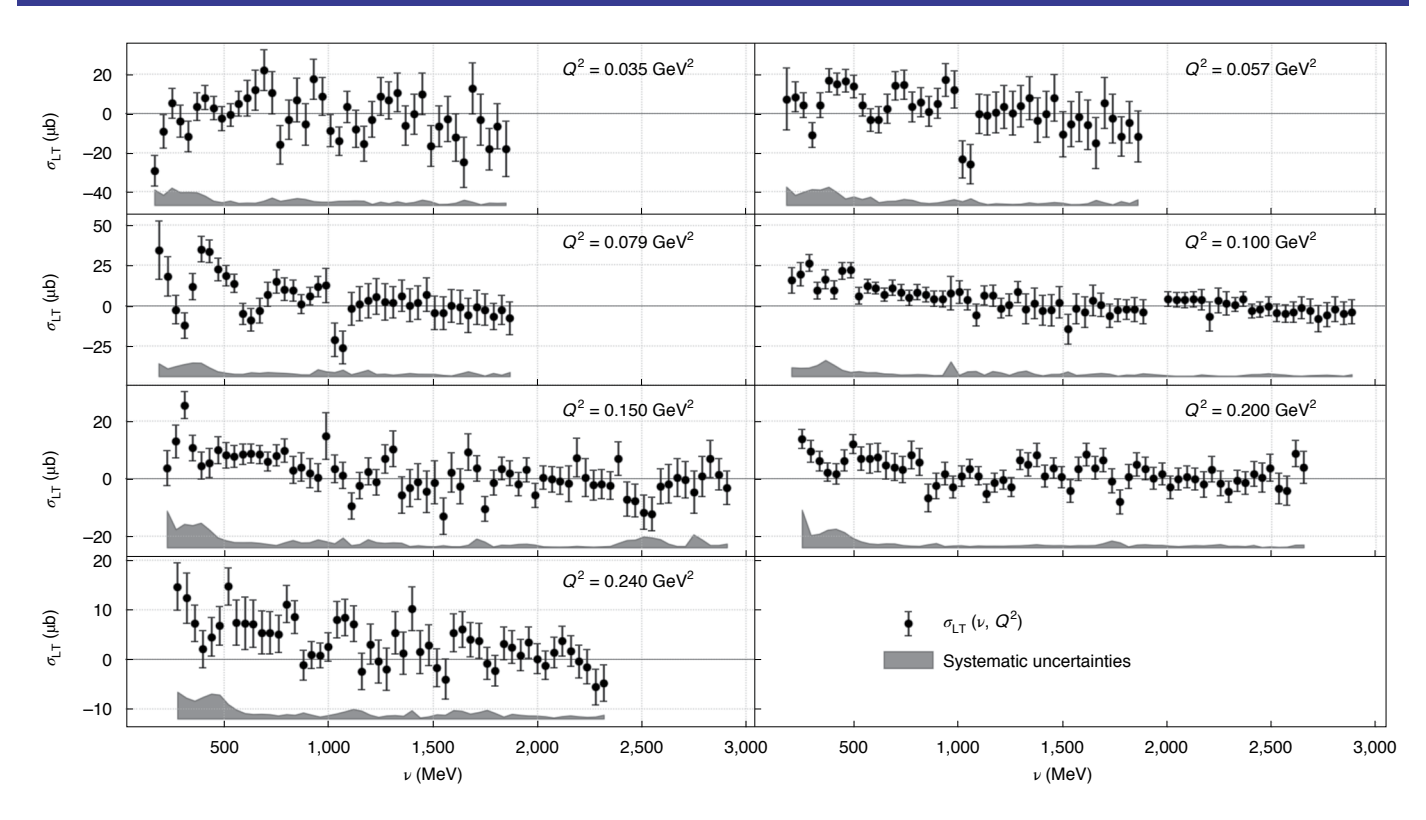


Fig. 3 | The longitudinal-transverse interference cross-section $\sigma_{LT}(\nu, Q^2)$ for ³He. The data are displayed at the Q^2 values at which they are integrated into $\delta_{LT}(Q^2)$ (equation (2)) or $I_{LT}(Q^2)$ (equation (5)). The error bars represent the statistical uncertainties. The systematic uncertainty is indicated by the band at the bottom of each panel. The nuclear corrections necessary to obtain the neutron information from the ³He data are applied after the integration. The prominent Δ(1232) contribution seen for $\sigma_{TT}(\nu, Q^2)$ in Fig. 2 is not present here, in agreement with the expectation that the role of Δ(1232) is suppressed in LT interference quantities.

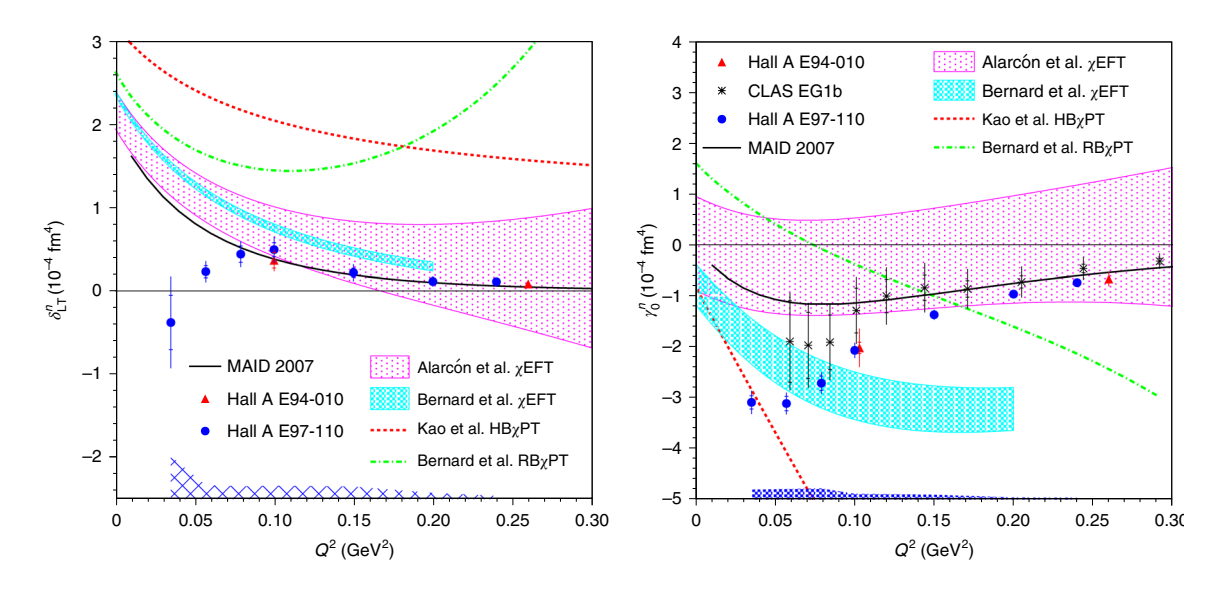


Fig. 4 | The generalized spin polarizabilities $\delta_{LT}^n(\mathbf{Q}^2)$ and $\gamma_0^n(\mathbf{Q}^2)$. Left: the generalized spin polarizability $\delta_{LT}^n(Q^2)$. The circles represent the results from experiment E97-110. They can be compared to earlier E94-010 data¹¹ (triangles) and theoretical calculations: the older χΕFT calculations of Bernard et al.¹² (dot-dashed line) and of Kao et al.¹³ (dashed line) in which the Δ resonance contribution is not included or included phenomenologically, the state-of-the-art calculations of Bernard et al.² (cyan band) and of Alarcón et al.⁴ (magenta band) that include the Δ, as well as the MAID model²¹ (black curve), which is a fit to world resonance data. For the E97-110 data, the inner error bars, sometimes too small to be visible, represent the statistical uncertainties. The outer error bars show the combined statistical and uncorrelated systematic uncertainties. The correlated systematic uncertainty is indicated by the band at the bottom. For the other experimental data, the error bars show the statistical and systematic uncertainties added in quadrature. Right: the generalized forward spin polarizability $\gamma_0^n(Q^2)$, using the same symbols as in the left panel. The asterisks represent the CLAS data²².

NATURE PHYSICS LETTERS

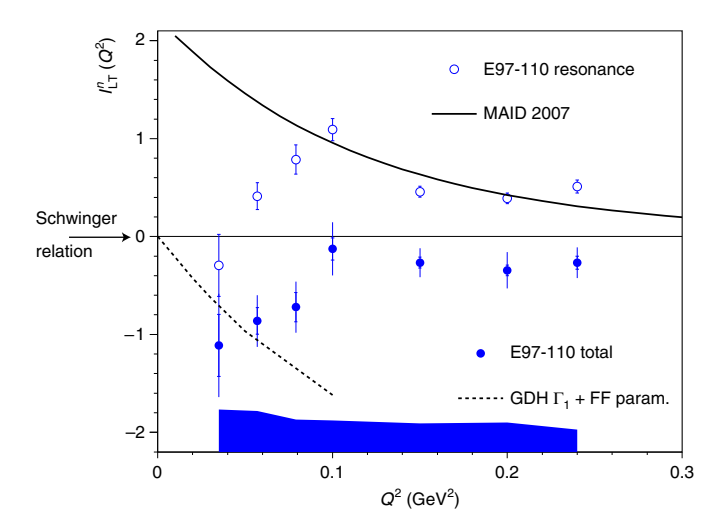


Fig. 5 | The Schwinger integral $I_{LT}^{n}(Q^2)$. The open symbols are our results without the large ν part of I_{LT} . The filled blue circles are our results for the full I_{LT} , using an estimate for the large ν contribution. The inner error bars represent the statistical uncertainties. The outer error bars show the combined statistical and uncorrelated systematic uncertainties. The correlated systematic uncertainty is indicated by the band. The Schwinger relation²³ for the neutron predicts that $I_{LT}^{n}(0) = 0$ at $Q^2 = 0$. The solid line shows the MAID model²¹, which is a fit to world resonance data (to be compared to the open symbols). The dashed line uses the GDH $(\Gamma_1)^{26,27}$ and Burkhardt–Cottingham³⁰ relations, together with an elastic form factor parameterization (FF param.)³¹, to obtain $I_{LT}^{n}(Q^2)$ for $Q^2 \rightarrow 0$.

relation²³, which has a similar definition but without ν^{-2} weighting in its integrand:

$$I_{\rm LT}(Q^2) \equiv \left(rac{M^2}{lpha\pi^2}
ight) \int_{
u_0}^{\infty} \left[\kappa_\gamma rac{\sigma_{
m LT}(
u,Q^2)}{Q
u}
ight]_{Q=0} {
m d}
u.$$
 (5)

Schwinger predicted that $Q^2 \to 0$ $I_{LT}(Q^2) \to \kappa e_t$, with κ the anomalous magnetic moment of the target particle and e_t its electric charge. This prediction is general; for example, it does not use χ EFT. $I_{\rm LT}(Q^2)$ has no ν^{-2} weighting, and therefore the large ν contribution to the integral is not negligible. As this contribution to the integral cannot be measured, a parameterization based on the model described in ref. 24 completed by a Regge-based parameterization25 for the largest ν part was used to extrapolate it. Our measurement of $I_{LT}^n(Q^2)$ is shown in Fig. 5. Our measurement of $I_{LT}^n(Q^2)$ without the Regge-based parameterization²⁵ for the large ν part (open symbols), which is suppressed in $\delta_{LT}(Q^2)$, displays a pattern similar to that of $\delta_{LT}^n(Q^2)$. The Gerasimov–Drell–Hearn (GDH) relation^{26,27} can be used to extrapolate our $I_{LT}^n(Q^2)$ to $Q^2 = 0$; provided that the GDH relation is valid, which is widely expected and supported by dedicated experimental studies²⁸, our data satisfy Schwinger's prediction that $I_{LT}^n(0) = 0$ (ref. ²³). Our trend contrasts with the MAID model and presumably the χEFT calculations, as MAID tracks those (Fig. 4). This suggests that the problem lies in the theoretical description of the neutron structure. The measured $I_{LT}(Q^2)$ displays a Q^2 behaviour similar to that of $\delta_{\rm LD}$ irrespective of the different ν weighting. Other integrals without ν^{-2} weighting that were formed using our data and reported in ref. 16 did not display the surprisingly strong disagreement with the predictions seen here. The values of γ_0^n , δ_{LT}^n and I_{LT}^n with their uncertainties are available in the Supplementary Information.

Our data indicate that both the TT and LT interferences of the electromagnetic field's components induce a clear spin precession of the neutron. All calculations and models predicted that the LT

term influence should intensify at small Q^2 , but our data reveal the opposite trend. This notable disagreement is perplexing as our measurements were done well into the domain where χ EFT is expected to describe reliably the nucleon properties, especially the 'gold-plated' δ_{LT} . Lattice QCD calculations of $\delta_{LT}(Q^2)$ are possible²⁹ but not yet available. Our data motivate such calculations as the measured generalized spin polarizabilities underline a current lack of reliable quantitative descriptions of the strong interaction at the nucleon-size scale.

Online content

Any methods, additional references, Nature Research reporting summaries, source data, extended data, supplementary information, acknowledgements, peer review information; details of author contributions and competing interests; and statements of data and code availability are available at https://doi.org/10.1038/s41567-021-01245-9.

Received: 8 January 2021; Accepted: 9 April 2021; Published online: 31 May 2021

References

- Bernard, V., Kaiser, N. & Meissner, U.-G. Chiral dynamics in nucleons and nuclei. Int. J. Mod. Phys. E 4, 193–346 (1995).
- Bernard, V., Epelbaum, E., Krebs, H. & Meissner, U.-G. New insights into the spin structure of the nucleon. *Phys. Rev. D* 87, 054032 (2013).
- Lensky, V., Alarcón, J. M. & Pascalutsa, V. Moments of nucleon structure functions at next-to-leading order in baryon chiral perturbation theory. *Phys. Rev. C* 90, 055202 (2014).
- Alarcón, J. M., Hagelstein, F., Lensky, V. & Pascalutsa, V. Forward doubly-virtual Compton scattering off the nucleon in chiral perturbation theory. II. Spin polarizabilities and moments of polarized structure functions. *Phys. Rev. D* 102, 114026 (2020).
- Deur, A., Brodsky, S. J. & de Téramond, G. F. The QCD running coupling. Prog. Part. Nucl. Phys. 90, 1–74 (2016).
- Deur, A., Brodsky, S. J. & de Téramond, G. F. The spin structure of the nucleon. Rep. Prog. Phys. 82, 076201 (2019).
- Gell-Mann, M., Goldberger, M. L. & Thirring, W. E. Use of causality conditions in quantum theory. *Phys. Rev.* 95, 1612–1627 (1954).
- Guichon, P. A. M., Liu, G. Q. & Thomas, A. W. Virtual Compton scattering and generalized polarizabilities of the proton. *Nucl. Phys. A* 591, 606–638 (1995).
- Hand, L. N. Experimental investigation of pion electroproduction. *Phys. Rev.* 129, 1834–1846 (1963)
- Chen, J.-P. Moments of spin structure functions: sum rules and polarizabilities. *Int. J. Mod. Phys. E* 19, 1893–1921 (2010).
- Amarian, M. et al. Measurement of the generalized forward spin polarizabilities of the neutron. *Phys. Rev. Lett.* 93, 152301 (2004).
- Bernard, V., Hemmert, T. R. & Meissner, U.-G. Spin structure of the nucleon at low-energies. *Phys. Rev. D* 67, 076008 (2003).
- Kao, C. W., Spitzenberg, T. & Vanderhaeghen, M. Burkhardt-Cottingham sum rule and forward spin polarizabilities in heavy baryon chiral perturbation theory. *Phys. Rev. D* 67, 016001 (2003).
- Hagelstein, F., Miskimen, R. & Pascalutsa, V. Nucleon polarizabilities: from Compton scattering to hydrogen atom. *Prog. Part. Nucl. Phys.* 88, 29–97 (2016).
- Alcorn, J. et al. Basic instrumentation for Hall A at Jefferson Lab. Nucl. Instrum. Methods Phys. Res. A 522, 294–346 (2004).
- 16. Sulkosky, V. et al. Measurement of the ³He spin-structure functions and of neutron (³He) spin-dependent sum rules at 0.035 ≤ Q² ≤ 0.24 GeV². Phys. Lett. B 805, 135428 (2020).
- Garibaldi, F. et al. High-resolution hypernuclear spectroscopy at Jefferson Lab, Hall A. Phys. Rev. C 99, 054309 (2019).
- 18. Ciofi degli Atti, C. & Scopetta, S. On the extraction of the neutron spin structure functions and the Gerasimov–Drell–Hearn integral from ³He(₹, e')X data. *Phys. Lett. B* **404**, 223–229 (1997).
- Deltuva, A., Fonseca, A. C. & Sauer, P. U. Momentum-space treatment of Coulomb interaction in three-nucleon reactions with two protons. *Phys. Rev.* C 71, 054005 (2005).
- Golak, J. et al. Proton polarizations in polarized ³He studied with the ³He (e, e-prime p) d and ³He (polarized-e, e-prime p) pn processes. *Phys. Rev. C* 72, 054005 (2005).
- Drechsel, D., Hanstein, O., Kamalov, S. S. & Tiator, L. A unitary isobar model for pion photo- and electroproduction on the proton up to 1 GeV. *Nucl. Phys.* A 645, 145–174 (1999).

LETTERS NATURE PHYSICS

- Guler, N. et al. Precise determination of the deuteron spin structure at low to moderate Q² with CLAS and extraction of the neutron contribution. *Phys. Rev. C* 92, 055201 (2015).
- Schwinger, J. S. Source theory viewpoints in deep inelastic scattering. Proc. Natl Acad. Sci. USA 72, 1–5 (1975).
- Adhikari, K. P. et al. Measurement of the Q² dependence of the deuteron spin structure function g₁ and its moments at low Q² with CLAS. *Phys. Rev. Lett.* 120, 062501 (2018).
- Bass, S. D., Skurzok, M. & Moskal, P. Updating spin-dependent Regge intercepts. Phys. Rev. C 98, 025209 (2018).
- Gerasimov, S. B. A sum rule for magnetic moments and the damping of the nucleon magnetic moment in nuclei. Sov. J. Nucl. Phys. 2, 430–433 (1966).
- Drell, S. D. & Hearn, A. C. Exact sum rule for nucleon magnetic moments. Phys. Rev. Lett. 16, 908–911 (1966).

- Helbing, K. The Gerasimov–Drell–Hearn sum rule. Prog. Part. Nucl. Phys. 57, 405–469 (2006).
- Chambers, A. J. et al. Nucleon structure functions from operator product expansion on the lattice. *Phys. Rev. Lett.* 118, 242001 (2017).
- Burkhardt, H. & Cottingham, W. N. Sum rules for forward virtual Compton scattering. Ann. Phys. 56, 453–463 (1970).
- Ye, Z., Arrington, J., Hill, R. J. & Lee, G. Proton and neutron electromagnetic form factors and uncertainties. *Phys. Lett. B* 777, 8–15 (2018).

Publisher's note Springer Nature remains neutral with regard to jurisdictional claims in published maps and institutional affiliations.

© The Author(s), under exclusive licence to Springer Nature Limited 2021

'William & Mary, Williamsburg, VA, USA. ²Thomas Jefferson National Accelerator Facility, Newport News, VA, USA. ³University of Virginia, Charlottesville, VA, USA. ⁴Duke University and Triangle Universities Nuclear Laboratory, Durham, NC, USA. ⁵Argonne National Laboratory, Lemont, IL, USA. ⁶Yerevan Physics Institute, Yerevan, Armenia. ⁷California State University, Los Angeles, Los Angeles, CA, USA. ⁸Massachusetts Institute of Technology, Cambridge, MA, USA. ⁹LPC Clermont-Ferrand, Université Blaise Pascal, CNRS/IN2P3, Aubière, France. ¹⁰Temple University, Philadelphia, PA, USA. ¹¹Florida International University, Miami, FL, USA. ¹²University of Maryland, College Park, MD, USA. ¹³Istituto Nazionale di Fisica Nucleare, Rome, Italy. ¹⁴Istituto Nazionale di Fisica Nucleare, Sezione di Bari and University of Bari, Bari, Italy. ¹⁵Longwood University, Farmville, VA, USA. ¹⁶University of Kentucky, Lexington, KY, USA. ¹⁷Istituto Superiore di Sanità, Rome, Italy. ¹⁸Rutgers, The State University of New Jersey, Piscataway, NJ, USA. ¹⁹Kharkov Institute of Physics and Technology, Kharkov, Ukraine. ²⁰Old Dominion University, Norfolk, VA, USA. ²¹University of New Hampshire, Durham, NH, USA. ²²Cairo University, Giza, Egypt. ²³University of Massachusetts Amherst, Amherst, MA, USA. ²⁴Kyungpook National University, Daegu, South Korea. ²⁵University of Saskatchewan, Saskatoon, SK, Canada. ²⁶DAPHNIA/SPhN, CEA Saclay, Gif-sur-Yvette, France. ²⁷Department of Modern Physics, University of Science and Technology of China, Hefei, China. ²⁸Randolph-Macon College, Ashland, VA, USA. ²⁹Jožef Stefan Institute, University of Ljubljana, Ljubljana, Ljubljana, Slovenia. ³⁶Norfolk State University, Norfolk, VA, USA. ³⁴LPSC, Université Joseph Fourier, CNRS/IN2P3, INPG, Grenoble, France. ³⁵Deceased: John M. Finn, Cornelis W. de Jager, Salvatore Frullani, Milan Potokar, Arun Saha, Patricia Solvignon, Ramesh Subedi. ²⁶e-mail: deurpam@jlab.org

NATURE PHYSICS LETTERS

Data availability

All experimental data that support the findings of this study are provided in the Supplementary Information or are available from J.P.C. (jpchen@jlab.org), A.D. (deurpam@jlab.org), C.P. (cpeng@jlab.org) or V.S. (vasulk@jlab.org) upon request.

Code availability

The computer codes that support the plots within this paper and the findings of this study are available from J.P.C. (jpchen@jlab.org), A.D. (deurpam@jlab.org), C.P. (cpeng@jlab.org) or V.S. (vasulk@jlab.org) upon request.

Acknowledgements

All authors are members of The Jefferson Lab E97-110 Collaboration. We acknowledge the outstanding support of the Jefferson Lab Hall A technical staff and the Physics and Accelerator Divisions that made this work possible. We thank A. Deltuva, J. Golak, F. Hagelstein, H. Krebs, V. Lensky, U.-G. Meißner, V. Pascalutsa, G. Salme, S. Scopetta and M. Vanderhaeghen for useful discussions and for sharing their calculations. We are grateful to V. Pascalutsa and M. Vanderhaeghen for suggesting a comparison of the data to the Schwinger relation. This material is based upon work supported by the United States Department of Energy, Office of Science, Office of Nuclear Physics under contract

DE-AC05-06OR23177 and by the United States National Science Foundation under grant PHY-0099557.

Author contributions

The members of the Jefferson Lab E97-110 Collaboration constructed and operated the experimental equipment used in this experiment. All authors contributed to the data collection, experiment design and commissioning, data processing, data analysis or Monte Carlo simulations. The following authors especially contributed to the main data analysis: J.P.C., A.D., C.P. and V.S.

Competing interests

The authors declare no competing interests.

Additional information

Supplementary information The online version contains supplementary material available at https://doi.org/10.1038/s41567-021-01245-9.

Correspondence and requests for materials should be addressed to A.D.

Peer review information *Nature Physics* thanks Mohammad Ahmed, Jan Friedrich and the other, anonymous, reviewer(s) for their contribution to the peer review of this work.

 $\textbf{Reprints and permissions information} \ is \ available \ at \ www.nature.com/reprints.$